Snowmelt duration controls red algal blooms in the snow of the European Alps

Leon Roussel, Marie Dumont, Simon Gascoin, Diego Monteiro, Mathias Bavay, Pierre Nabat, Jade Abdelattif Ezzedine, Mathieu Fructus, Matthieu Lafaysse, Samuel Morin, et al.

PNAS RESEARCH ARTICLE | EARTH, ATMOSPHERIC, AND PLANETARY SCIENCES
ENVIRONMENTAL SCIENCES

Snowmelt duration controls red algal blooms in the snow of the European Alps

Léon Rousset[a,1,2], Marie Dumont[a,1], Simon Gascoin[b], Diego Monteiro[a], Mathias Bavay[c], Pierre Nabat[d], Jade Abdellatif Ezzedine[e], Mathieu Fructus[a], Matthieu Lafaysse[a], Samuel Morin[d], and Eric Maréchal[e]

Affiliations are included on p. 9.

Edited by James Randerson, University of California, Irvine, CA; received January 17, 2024; accepted July 16, 2024

Algae populate multiple habitats, including snow and ice, where they can form red blooms. These decrease snow albedo, accelerating snowmelt and potentially feeding back on snow and glacier decline caused by climate change. Quantifying this feedback requires the understanding of bloom evolution with climate change. Little, however, is known about the drivers of red snow blooms. Here, we develop an algorithm to analyze 5 y of satellite data from the European Alps and separate bloom occurrences from similarly colored Saharan dust depositions. In a second step, we combine the occurrences of blooms with meteorological data and snow simulations to identify the drivers of blooms. Results show that the upward migration of algae from the ground and blooming requires the presence of liquid water throughout the whole snow column for at least 46 d. Our limited data suggest that moderate dust amounts provide nutrients favorable to bloom, whereas large dust amounts hasten snowmelt and reduce its duration below the threshold required for blooming. Over the period studied, blooms cover 1.3% of the area above 1,800 m elevation, advancing the snow melt-out date by 4 to 21 d in these areas. Under warmer climates, maximum snow mass will decrease whereas snowmelt duration, that controls algal blooms' occurrences, is less sensitive to global temperature increase. In this respect, the impact of bloom on snowmelt will either remain stable (RCP4.5) or decrease (RCP8.5). Algal blooms in the Alps therefore do not constitute a positive climate feedback.

snow | algae | melt | climate change | Alps

Significance

In late spring, the algae *Sanguina nivaloides* sometimes colors the snow, forming red blooms commonly known as "watermelon snow." Algal blooms accelerate snowmelt by reducing snow albedo. Since the environmental triggers of the blooms are not well identified, reliable projections of the blooms' evolution with climate change and their future contribution to the snowmelt cannot be assessed. By combining snowpack simulations and a multitemporal atlas of blooms in the European Alps, we show that a long duration of snowmelt allows algal development and promotes a high occurrence of blooms. The duration of snowmelt, and thus the bloom occurrence is projected to remain stable or decrease with climate change. Hence the algal contribution to snowmelt will not increase with climate warming.

Algae are found not only in lakes and oceans but also on land in snow cover. In these cold environments, they play an important role in hydrological and geochemical processes (1, 2). When conditions are favorable, algae form blooms, i.e., the rapid proliferation of algal populations. On snow, these blooms may take various colors, such as red (Fig. 1 *A* and *B*), brown, and green, depending on the species (3). In the Alps, snow algae are present on snow overlying glaciers (e.g., 4) and also outside of glaciers on seasonal snow (e.g., 5), where the predominant species is a green alga (Chlorophyta) named *Sanguina nivaloides*. This alga produces red pigments, known as carotenoids, therefore forming red blooms near the snow surface in spring and summer (6).

By lowering the albedo of snow and ice surfaces, algae accelerate melt (7–10), which can cause up to 3 cm of additional snow meltwater equivalent on North American glaciers (11). Snow algae interact with other living organisms in their ecosystem (3, 12, 13). Indeed, snow is a unique habitat that is mostly populated by microorganisms. As primary producers, photosynthetic organisms capture atmospheric CO_2 and produce organic molecules to form the base of trophic networks. As a consequence, the complete equilibrium of snow and ice microbial ecosystems relies on these algae (14). The biomass generated by snow algae feed bacteria (12), fungi (13), and other heterotrophs in the snowpack, on the snow surface in the form of cell-rich biofilms, and in the soil following snowmelt.

Snow algal blooms have been documented over short periods of time at some locations in Alaska, Canada, Greenland, California, and Antarctica (1, 11, 15–17) and in only a few places in the European Alps (4, 5). However, little is known about the processes that cause snow algae to bloom. The main drivers are expected to include nutrients (6, 18, 19), liquid water, and light (16), but their respective contributions and importance are unclear. While algal blooms in the oceans were shown to increase significantly in the 21st century (20), the possible future evolution of red snow blooms and their contribution to melt in response to climate change is difficult to ascertain in the absence of knowledge about red snow bloom drivers.

The authors declare no competing interest.

This article is a PNAS Direct Submission.

[1] L.R. and M.D. contributed equally to this work.

[2]To whom correspondence may be addressed. Email: leon.roussel@meteo.fr.

This article contains supporting information online at https://www.pnas.org/lookup/suppl/doi:10.1073/pnas.2400362121/-/DCSupplemental.

Published September 23, 2024.

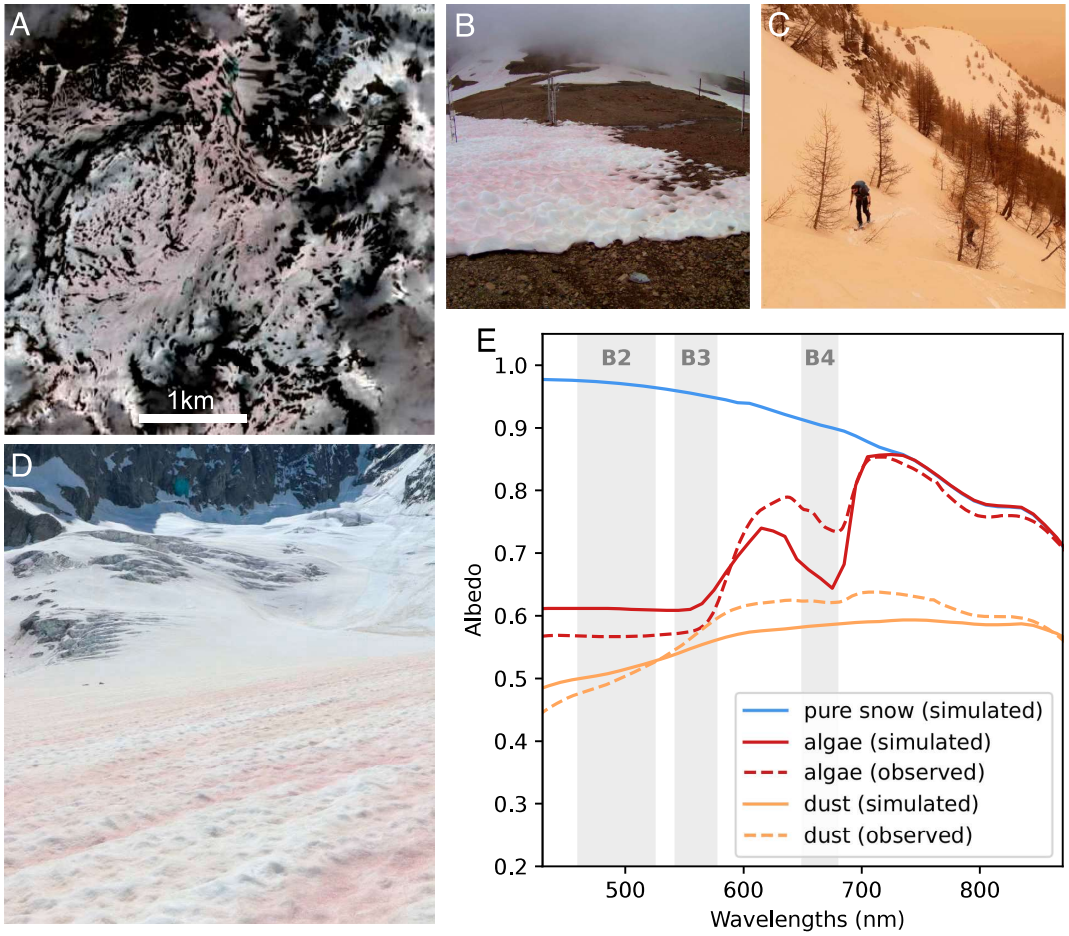

Fig. 1. Effect of mineral dust and algae on snow color and reflectance. (*A*) Sentinel-2 satellite true color image of a large red snow bloom, Vanoise, 19/06/2018. (*B*) Red snow bloom at Col du Lac Blanc, French Alps, 26/06/2018, credits: Météo-France. (*C*) Saharan dust on snow during a major deposition event, Queyras, French Alps, 06/02/2021, credits: Bertrand Cluzet. (*D*) Mixture of Saharan dust and red snow bloom on the Léchaux glacier, Mont-Blanc area, 30/06/2020, credits: Bruno Jourdain. (*E*) Simulated and observed spectral albedo for pure snow, snow containing Saharan dust, and snow containing algae. Simulations were performed with the SNICAR model (27), and the parameters are described in *Materials and Methods* (red line: no dust, algae concentration of 10^4 cells/mL, yellow line: no algae, dust concentration of 1,000 ppm for two size bins (5 to 10 and 10 to 100 μm), blue line: no dust, no algae). The observed spectra are from ref. 28. The Sentinel-2 spectral bands are highlighted in gray.

Changes in the snow color due to red algal blooms make them detectable through optical satellite imagery (11, 16, 21–23) (Fig. 1*A*). In the European Alps, the frequent deposition of Saharan dust (24, 25) turns snow orange or red, which can be confused with the color of algal blooms (Fig. 1 *C* and *D*). Consequently, existing bloom detection methods based on remote sensing data are inadequate (26).

Here, we combined high-resolution remote sensing and snowpack modeling to decipher the potential drivers of red algal blooms in the European Alps over a region of 94,200 km^2 spanning from France to Austria. To do so, we developed and used a method to map red snow blooms from optical satellite imagery in regions also impacted by mineral dust deposition. Our analysis covered the five spring and summer seasons from 2018 to 2022, featuring contrasting meteorological, snow, and dust deposition conditions. The resulting dataset is a multiyear atlas of snow algal blooms over a large region, spanning a wide range of climatic and topographic conditions. This allowed us to identify the key processes that trigger snow algal blooms. Based on these findings, we can assess the potential evolution of snow algal blooms under future climate conditions.

Results and Discussion

Where and When do Red Snow Blooms Occur in the European Alps? We identified the occurrence of algal blooms at a 10 m horizontal resolution across the European Alps from Sentinel-2 satellite images (29). We combined Sentinel-2 surface reflectance data and snow cover products (30) to apply an algal bloom detection algorithm based on three spectral bands (blue, green, and red) for which the responses of snow containing dust and snow containing algae are slightly different (Fig. 1*E*; *Materials and Methods*). We used every image acquired between 1 May and 15 August from 2018 to 2022. We estimated the accuracy of the method to 98.6% using 4,600 webcam images available in the Alps (*SI Appendix*, Fig. S1 for the locations of the six webcams). Our method was designed to reduce false positive cases as much as possible; as a consequence, it only detects intense algal blooms and does not classify blooms when dust and algae are mixed, as illustrated in Fig. 1*D*.

We identified approximately 5.5 million pixels with algal blooms over the 5-y study period (at 10 m horizontal resolution). Algal blooms were unevenly distributed in the European Alps (Fig. 2). We found areas of high bloom density in Vanoise,

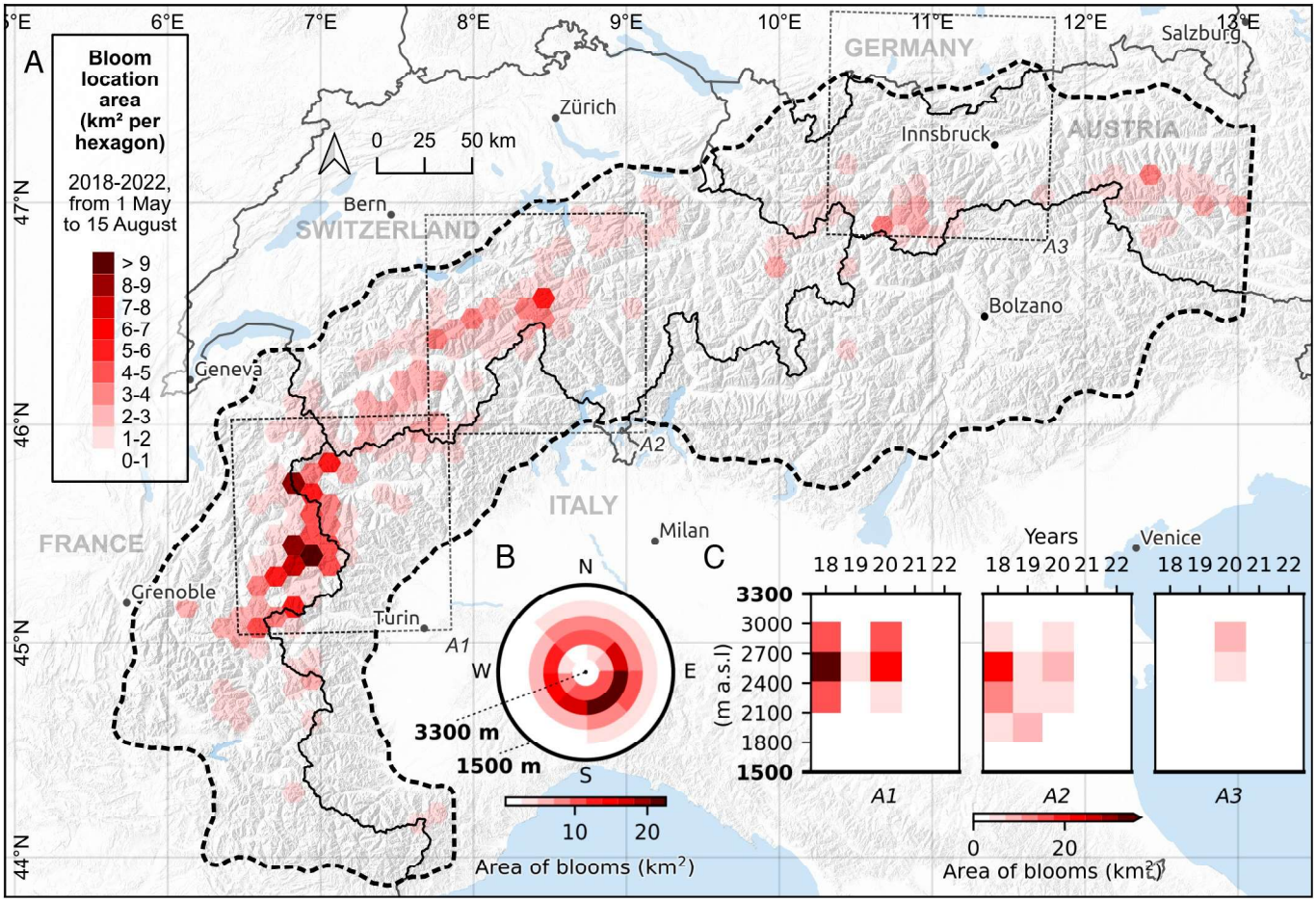

Fig. 2. Areas of red algal blooms in the snow in the European Alps. (*A*) Maximum area covered by blooms over the studied period from 1 May to 15 August for the years 2018 to 2022. The studied area is delimited with a dashed black line (*Materials and Methods*). The maximum areas covered by blooms were aggregated by hexagons with a surface area of 96 km^2. (*B*) Areas of detected algal bloom by elevation and aspect classes over the same period as Panel *A*, and for the 3 specific zones (A1, A2, and A3) depicted in Panel *A*. Areas are grouped by 300 m elevation bins from 1,500 (outside circle) to 3,300 m a.s.l. (inside dot). (*C*) Areas of algal bloom per year and elevation bin for the three specific zones (A1, A2, and A3) depicted in Panel *A*. Background map from OpenStreetMap.

Tarentaise, and Maurienne in the northern French Alps (zone A1), Oberland and Valais in Switzerland (zone A2), and, to a lesser extent, Ötzal and Hohe Tauern in Austria (zone A3). Furthermore, we found that algal blooms occurred preferentially in a specific elevation range since 94% of bloom retrievals in zones A1, A2, and A3 were in the range 1,800 to 3,000 m above sea level (a.s.l.), 2.5% in the range 1,500 to 1,800 m a.s.l., and 3.5% only above 3,000 m a.s.l. (Fig. 2 *B* and *C*). Algal blooms followed the snow line elevation from May onward, i.e., they were located near the lowest edge of the snow cover (*SI Appendix*, Fig. S2). The detection count per month was greater in June than in May, July, and August in the three zones (71% of the retrievals in June for zone A1, 54% for zone A2, and 43% for zone A3). The blooms occurred preferentially on south- to east-facing slopes (Fig. 2*B*). In zones A1, A2, and A3, 62 % of the bloom retrievals were found on NE to SW slopes, and 35 % were found on E to S slopes. Blooms were found to occur preferentially on areas of gentle slopes, typically lower than 25 degrees (*SI Appendix*, Fig. S3). Only 5.5 % of the bloom retrievals were located on glaciers.

The occurrence of red algal blooms showed great interannual variability: 2018 and 2020 were years with a large number of occurrences, while we observed fewer occurrences for the other 3 y of the study (2019, 2021, and 2022) (Fig. 2*C* and *SI Appendix*, Fig. S2). In zones A1, A2, and A3, we identified approximately 2.7 million pixels with algal blooms in 2018 and 2020, in contrast to the 0.7 million pixels identified in 2019, 2021, and 2022. However, from one year to the next, most of the blooms occur at the same location or in close vicinity. For example, in zone A1 (Fig. 1*A*, 1.5 million retrievals), 7.2% of the blooms were at the exact same location from one year to the other, and 50% of the blooms were located within a distance of less than 100 m from one year to the next. Zone A2 contains many glaciers, including Kander Neve, Aletsch Glacier, Rhône Glacier, and Gorner Glacier. In this whole zone, 5.3% of the blooms were at the exact same location from one year to the other, and when restricted to glacier areas, 13.2% of the blooms were at the exact same location from one year to the other. This interannual stability of the bloom locations on glaciers was, for example, evident on Aletsch Glacier in Switzerland (*SI Appendix*, Fig. S4) and was found to be higher for snow on glaciers than for snow outside glaciers. In summary, algal bloom locations are not randomly distributed and tend to repeat at the same location or within close distances to the same location from one year to the next, with substantial interannual variability.

What Are the Drivers of Red Algae Snow Blooms? Nutrients, liquid water, and light are believed to control snow algal abundance (16). The high interannual variability of bloom occurrence (Fig. 2*C*) suggests that the occurrences are linked

to the interannual variability of the meteorological and snow conditions. Thus, to investigate the various drivers of red algal blooms in the Alps and their respective importance, we combined our bloom dataset with a reanalysis of snow and meteorological conditions, together with estimates of mineral dust deposition surface fluxes (31). Our approach requires accounting for the snow cover properties layer by layer. Hence, we performed this analysis in the French Alps and Switzerland, where such information is available (*Data, Materials, and Software Availability*) from detailed snow models, Crocus in France (32) and SNOWPACK in Switzerland (33). We selected 40 points where a bloom was detected at least once during the study period in areas with a high number of total detection (27 points in the French Alps and 13 points in Switzerland). These points are located between 2,200 m and 3,000 m a.s.l. (*SI Appendix*, Fig. S1). The selected number of points results from a trade-off between the spatial resolution of the available meteorological and snow conditions, and the need to have a sufficiently large sample. For each of these points, we analyzed the snow, meteorological, and dust conditions as a function of the bloom occurrences.

Among the snow and meteorological variables that we explored (*SI Appendix*, Table S1), only a few exhibited large correlations with the presence of blooms, and all of them were related either to snow water equivalent (mass of snow) or liquid water in snow (*Materials and Methods*). Therefore, we introduced two indicators: i) the snowmelt duration, i.e., the number of days for which the snow water equivalent strictly decreases between the date of the maximum snow water equivalent and the date of complete melt-out, and ii) the persistence of liquid water, i.e., the number of days with a fully wet snowpack (when layers containing liquid water account for more than 90% of the snowpack total thickness) between the date of the maximum snow water equivalent and the date of complete melt-out. Both indicators were higher when blooms occurred (Fig. 3*A*). This suggests that the development of algal blooms is conditioned by a long duration of snowmelt, longer than 46 d (Q1 of snowmelt duration in Fig. 3*A*) and by the presence of liquid water in the full column of snow for a sufficiently long period, here longer than 42 d (Q1 of the persistence in liquid water in Fig. 3*A*). Both indicators are closely related, as snowpack melt is often connected to a fully wet column of snow. In our study, a long snowmelt duration was related to a high snow mass (Fig. 3*B*) and an early onset of melt (Fig. 3 *D* and *E*).

Based on these 5 y, we found that none of the blooms occurred when the snowmelt duration was less than 25 d. On average, the snowmelt duration should last for 54 ± 12 d, and the liquid water should persist for 49 ± 13 d for intense snow algal blooms to be detected (medians and SD in Fig. 3*A*). Our results fall in line with several studies arguing that liquid water in snow cover over a sufficiently long time period could trigger snow algal blooms, such as on glaciers (16). It was also observed (17) that green algae could typically develop in wet snow at the boundary between recent snow at the surface of the snowpack and the older firn. Overall, this suggests that the presence of liquid water in snow for a sufficiently long period of time is a key driver of red-colored blooms in alpine snow.

Liquid water in snow is necessary for algae for two reasons. First, nutrients are released when ice melts. Second, snow algal species, including *S. nivaloides*, are postulated to migrate during a motile flagellated cell stage in the interstitial water within the snow (1, 34, 35). The literature mentions that blooms of *S. nivaloides* may germinate locally in the same areas year after year or might be dispersed by wind (36, 37). In the case of the European Alps, our analysis indicates that they mostly germinate locally in the same areas year after year and that airborne dispersion seems to be limited. Algae may be able to migrate upward depending on the light conditions and start proliferating and producing pigments when liquid water is present in the snowpack. It has been suspected (3) that regardless of the snow depth value, algal blooms can develop as long as the snowmelt time period is long enough to enable algae proliferation. However, previous studies did not quantify what "long enough" means. Our study concurred with this hypothesis and showed that for the European Alps, the snowmelt duration should typically be longer than 46 d (Q1 in Fig. 3*A*). In addition, the quasiabsence of blooms above 3,000 m a.s.l., which roughly corresponds to the elevation above which the ground is permanently frozen in the European Alps (38), suggests that the snow algae persist in environments where the ground is not frozen. This is in line with the recent observation that *S. nivaloides* cysts lose their photosynthetic capacity after freezing (6).

Nutrients are also considered in some cases to be the limiting factor for algae proliferation (16). These nutrients include phosphorus and potassium, which are present in Saharan dust (25, 39). We found a clear difference in dust deposition amounts for the years when a bloom was detected and those without blooms (Fig. 3*C*). In contrast, no bloom was observed in years with minimum or maximum dust deposition. All blooms occurred for years where the dust deposition was close to the local mean over the 5 y. This suggests that nutrients might be a limiting factor for low dust deposition years, in line with recent observations (6) at Vallon de Roche Noire and Mont Brévent, both sites located in France. For high dust years, the snow melts faster (8, 24, 40) and bloom proliferation may be limited when the mass of snow is not sufficient. However, these statements should be considered with caution, considering the limited number of years of the study and the limited accuracy of our detection method for blooms mixed with a high amount of dust.

In summary, our analysis suggests that in the European Alps, the development of red algal blooms in snow is strongly conditioned by the persistence of liquid water in the snowpack for a sufficient amount of time. In addition, we observed that blooms are unlikely to develop when the ground under the snow is permanently frozen. We also found that blooms occur only when dust deposition exceeds a minimum amount. While this suggests that blooms occur when two conditions are simultaneously met: i) wet snow conditions for a sufficiently long time together with ii) sufficient dust deposition input, due to the limitations of our detection method in cases of high dust content mixed with algae, it is difficult to make firm conclusions about the contribution of dust to algae proliferation. A sufficiently long wet snow time period appears to be a necessary condition regardless of the role of dust deposition.

Implications. By lowering the snow albedo, red blooms can highly accelerate snow melting (7) over large areas (11). Over the 5 y of our study, blooms were detected over a total area of 564 km^2, which is 1.3% of the total area above 1,800 m a.s.l. In 2018, both zones A1 and A2 presented their maximum areas covered by blooms over the 5 y of the study. These maxima were 93.8 km^2 over zone A1 and 46.7 km^2 over zone A2 (1.4% and 0.6% of the area above 1,800 m a.s.l. of each zone). Zone A3 exhibited this maximum in 2020 with 18.9 km^2 (0.5% of the area above 1,800 m a.s.l. of zone A3). In the area with the highest density of bloom detection (the darkest hexagon in

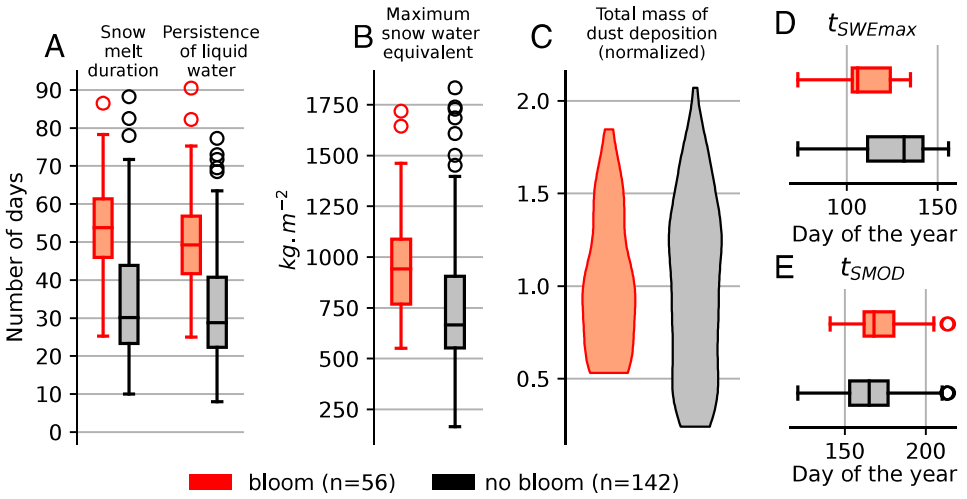

Fig. 3. Snow properties influence the occurrence of red algal blooms. (*A*) Boxplots of the snowmelt duration and persistence of liquid water for the 40 locations in the French and Swiss Alps and for the 5 y of the study for years with algae detection (red) and without algae detection (black). The snowmelt duration and persistence of liquid water were longer in cases where algae were detected (respectively *P*-value $= 1.3 \cdot 10^{-14}$ and *P*-value $= 4.9 \cdot 10^{-14}$ with one-sided Student's *t* test). (*B*) Same as Panel *A* with the maximum snow water equivalent, which was higher when an algal bloom was detected at the same location (*P*-value $= 2.2 \cdot 10^{-5}$ with one-sided Student's *t* test). (*C*) Dust deposition for each snow season, normalized at each location (*Materials and Methods*) and plotted using `violinplot` from `matplotlib`. Both violin plots are an estimation of the probability density function of the normalized dust content, i.e., the width on the *x* axis is a continuous approximation of data point frequency. (*D* and *E*) Boxplot of the dates of the maximum snow water equivalent (t_{SWEmax}) and the snow melt-out date (t_{SMOD}) over the same years and locations as Panel *A*. All boxes in the figure show the quartiles of the distribution. The upper bound for the upper whiskers extends to a last value less than $Q3 + 1.5 \times (Q3 - Q1)$, and the lower bound for the lower whiskers extends to a first value greater than $Q1 - 1.5 \times (Q3 - Q1)$. Outlier points are those past the end of the whiskers.

Fig. 2), within a snow-covered area of 60.4 km^2, the surface of the detected blooms was at a maximum of 5.5 km^2. This means that at most 9% was covered by red blooms. These areas would exhibit a decrease in the broadband snow albedo of 0.17 (Fig. 1; *Materials and Methods*) and would thus melt faster. For snow on glaciers, red blooms were detected, and the area with at least one bloom detected was equal to 31.6 km^2, which is 1.6% of the glaciated area. Intense bloom durations, identified both from satellite images and webcams, range between 18 and 30 d, and higher values are found on snow overlying glaciers. The associated increase in melting for bloom areas is thus at most 83 cm water equivalent (*Materials and Methods*). Thus, the maximum melt enhancement due to algal blooms for the total glaciated area is 13.4 mm water equivalent. For seasonal snow cover, we estimate that in areas where blooms are present, the snow melt-out date is advanced by 4 to 21 d. This provides an upper bound of the impact of red blooms on snowmelt in the European Alps.

However, two limitations of the study can influence these upper bounds. First, our method only detects intense blooms and does not detect blooms in cases of high dust content. The impact of this limitation is likely weak here since only intense blooms not mixed with dust have a very high impact on snowmelt. Second, the spatial resolution of Sentinel-2 images is limited to 10 m. Past studies (41) have shown that using higher-resolution satellite images, typically with one-meter horizontal resolution, can lead to retrieved bloom areas 17 times larger in regions with a high bloom density. Such high-resolution images are, however, not available for the areas and dates of interest. Finally, it is also important to note that this study addressed the role of red-pigmented cells of *S. nivaloides* populating melting snow. Other species can also form blooms, in particular *Ancylonema* species at the ice surface of glaciers, marked by the accumulation of a purple pigment, purpurogallin, which is more difficult to discriminate and detect from satellite images (4). We believe that, due to this difficulty in detection, the role of *Ancylonema* is overlooked.

Global warming is expected to impact the snow algal population. However, the limiting factor for bloom occurrences varies from one region to another since algae populate environments around the world with different topographies, solar radiation, nutrient inputs, and different ecosystems (1). As a consequence, the response of algae to climate change may differ by region. While larger snow algal blooms are expected in Antarctica (17) and the development of algae is expected on flat snow-covered topography such as Antarctica and Greenland (16), the future of the current snow algae in Europe is currently unknown.

We assessed future changes in snow conditions relevant to algal blooms under warmer climate conditions in the French Alps based on adjusted regional climate model (RCM) projections driven by global climate model (GCM) projections (*Materials and Methods*). The analysis of these simulations, illustrated in Fig. 4, indicates a progressive decline in the annual snow water equivalent maximum at 2,400 to 2,700 m a.s.l. (Fig. 4 *B* and *D*), an elevation range prevailing for algal bloom occurrence (Fig. 2*C*), both for the very high emission scenario (RCP8.5) and intermediate emission scenario (RCP4.5). Nonetheless, snowmelt duration appears to be less sensitive to climate change at those elevations; indeed, it does not decrease until 2050 (Fig. 4 *A* and *C*). In the RCP4.5 scenario, the snowmelt duration does not decrease after 2050 for elevations above 2,100 m a.s.l. (*P*-values in *SI Appendix*, Table S4). The decline in the snow water equivalent annual maximum is probably balanced by a slower melt rate in these cases (42). After 2050, snowmelt duration values are projected to start to decrease above 2,100 m a.s.l. for the RCP8.5 scenario. Hence, in the second part of the 21st century for RCP8.5, intense algal blooms may be less frequent at elevations where we observe them today. Snow algae may then find an appropriate environment at even higher elevations (e.g., above 3,000 m a.s.l.), which, however, represents a much smaller surface area, approximately five times smaller than the area in the range 2,500 to 3,000 m a.s.l. Overall, the area

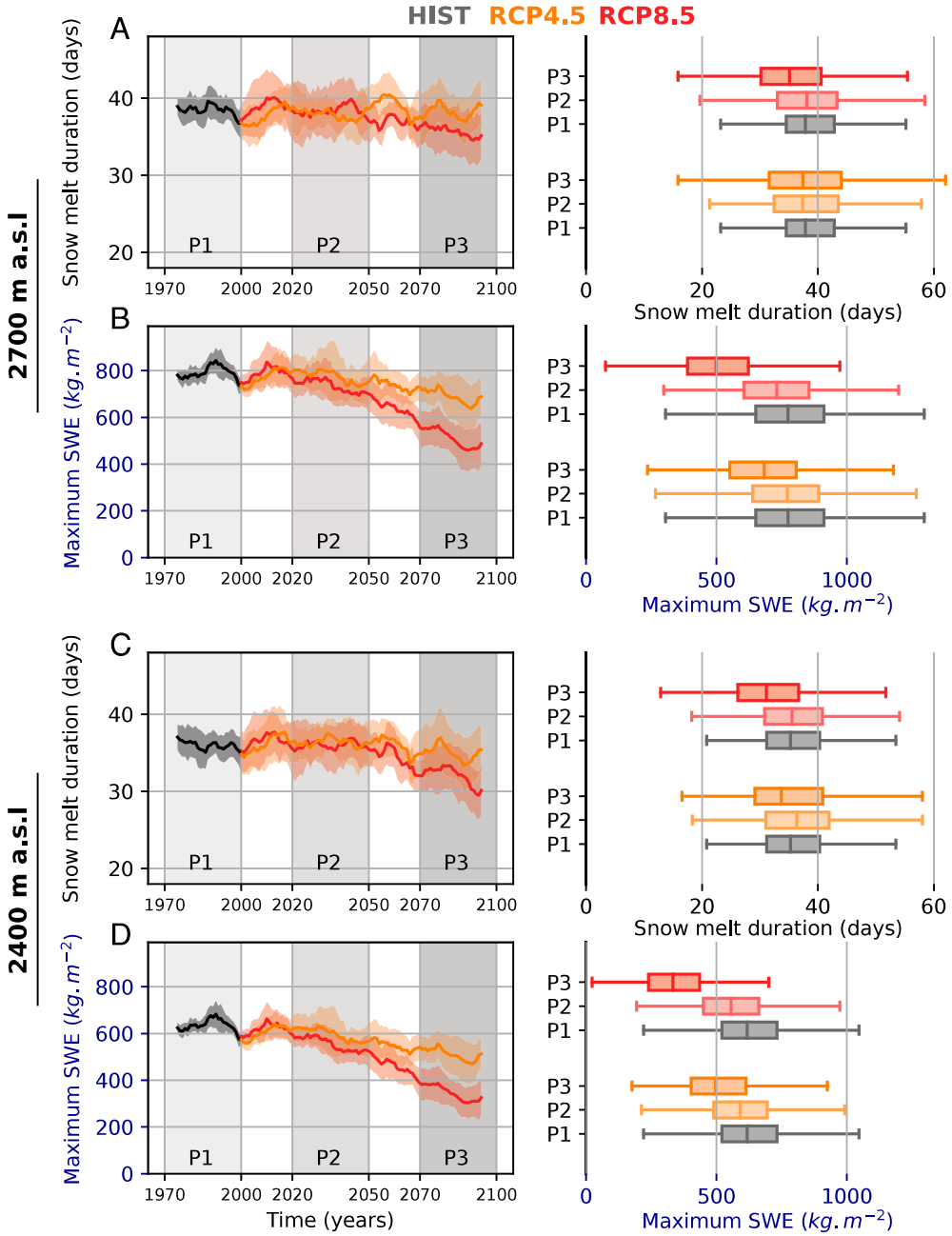

Fig. 4. Climate projections of snowmelt duration at 2,700 m a.s.l. (*A*), maximum snow water equivalent at 2,700 m a.s.l. (*B*), snowmelt duration at 2,400 m a.s.l. (*C*), maximum snow water equivalent at 2,400 m a.s.l. (*D*) in the French Alps for historical simulations (HIST in gray) and two future scenarios (RCP8.5 in red, RCP4.5 in orange). Fifteen adjusted GCM/RCM model pairs were used (*Materials and Methods*). *Left column* 10-y moving average (±5 y) over the 15 GCM/RCM pairs for each scenario. The colored shaded areas represent the 10-y moving average of one SD from the mean. Year n refers to the winter between years n and n+1. *Right column* Each box is built with 330 values (15 GCM/RCM pairs, 30 y corresponding to time periods P1, P2, or P3 in gray in the *Left* panels). All boxes show the quartiles of the distribution. The upper bound for upper whiskers extends to a last value less than $Q3 + 1.5 \times (Q3 - Q1)$, and the lower bound for lower whiskers extends to a first value greater than $Q1 - 1.5 \times (Q3 - Q1)$. Outlier points are not shown.

of favorable conditions for snow algal blooms is expected to be markedly smaller.

The future of snow algae in the European Alps is thus more constrained than in other regions of the world. Indeed, a declining snow cover could induce a rarefaction of these species for the very high emissions scenario. Hence, the evolution of red snow algae ecosystems in the European Alps will depend on future emission scenarios. The postulated extinction of *S. nivaloides* and other microalgae is likely to have critical and still unknown impacts on snow microbiota, and also on soil and other ecosystems connected via hydrological networks.

Materials and Methods

Sentinel-2 Images. We identified the occurrence of algal blooms at a 10 m resolution across the European Alps from Sentinel-2 mission data (29). Sentinel-2 images were provided for 12 spectral bands with a revisit time of at most 5 d. We combined Sentinel-2 surface reflectance and snow cover products to apply a machine-learning algorithm for algal bloom detection. We used every image acquired between 1 May and 15 August from 2018 to 2022 over a region of 94,200 km^2 corresponding to 19 Sentinel-2 tiles.

Surface Reflectance and Snow Mask. Surface reflectances were computed from Sentinel-2 data using MAJA (MACCS-ATCOR Joint Algorithm, with MACCS

standing for Multisensor Atmospheric Correction and Cloud Screening, and ATCOR standing for Atmospheric and Topographic Correction), a state-of-the-art level-2A processor that performs the correction of top-of-atmosphere reflectances to bottom-of-atmosphere reflectances (43). MAJA also computes a cloud mask (44). We selected these level-2A products because the MAJA processor is fully adequate in terms of surface reflectance and cloud masking accuracy (45, 46). The snow products were routinely derived from the same level-2A products using LIS software (Let It Snow) (30). The accuracy of snow detection from the MAJA-LIS pipeline against a large sample of in situ measurements across Europe was 94% (47). The study region was covered by tiles 31TGM, 31TGL, 31TGK, 31TGJ, 32TLS, 32TLR, 32TLQ, 32TLP, 32TMT, 32TMS, 32TMR, 32TNT, 32TNS, 32TNR, 32TPT, 32TPS, 32TPR, 32TQT, and 32TQS (*SI Appendix*, Fig. S1).

Study Domain. We defined the study domain based on prior knowledge that algae are always observed at elevations higher than 1,500 m a.s.l. (5). We extracted the Sentinel-2 pixels above this elevation within the Alpine Convention perimeter (48) and smoothed the resulting mask by erosion-dilatation (Fig. 2, dotted black line). Only a small fraction of the domain in the easternmost part of the Alps was not processed due to the unavailability of Sentinel-2 level-2A products.

Snow Reflectance Simulations. To simulate the albedo of snow containing dust and algae, we used the online two-stream radiative transfer model SNICAR (27). Different input parameters are required: the incident radiation characteristics, snowpack properties, properties of light-absorbing particles, and snow algae (49). The following parameters are the same for all simulations unless otherwise stated: sun zenith angle of 30°, snow thickness of 100 m, snow density of 400 kg m^{-3}, snow optical radius of 1 mm, dust sizes (0.1 to 1.0) μm, (1.0 to 2.5) μm, and (2.5 to 5.0) μm set to 0 ppm, algae radius set to 20 μm, chlorophyll-a to 0.005 %, chlorophyll-b to 0.005 %, photoprotective carotenoids to 0.1 % and photosynthetic carotenoids to 0.05 % (see next section for the justification of these fractions). These pigment fractions correspond to the dry cell mass fraction. Dust sizes (5.0 to 10.0) μm and (10.0 to 100.0) μm according to the size of Saharan dust samples measured in the Alps (39) vary by [0; 100; 200; 300; 500; 1,000; 2,000] ppm and algae concentrations vary by in [0; 5,000; 10,000; 20,000; 50,000; 100,000; 200,000] cells/mL. A total of 42 simulations were thus performed. For mixed cases, i.e., for snow containing both dust and algae, we defined the fraction of algae (*SI Appendix*, Fig. S7), η_a as:

$$\eta_a = \frac{\Delta\alpha_{\text{alg}}}{\Delta\alpha_{\text{alg}} + \Delta\alpha_{\text{dust}}}, \quad [1]$$

where $\Delta\alpha_{\text{alg}}$ is the reflectance difference between the spectrum with algae only and the spectrum of pure snow in band 1 (Fig. 1), and $\Delta\alpha_{\text{dust}}$ in the same but for dust only.

Spectral Properties of Algae. Algae light absorption in the snowpack is mostly characterized by the absorption of two pigments, photosynthetic and photoprotective carotenoids, which mainly absorb at 300 to 550 nm, and chlorophyll (a and b), which mainly absorb at 300 to 510 and 630 to 700 nm. In this work, we investigated mostly the presence of *S. nivaloides* (5). To link remote sensing observations with actual field measurements, red snow was collected aseptically on June 14, 2022, from a snowfield at Brevent (2,469 m a.s.l; 45.93402 N and 6.83654 E). The sampling site corresponded to melting seasonal snow located in the alpine zone. The sample originated from a pure red algae bloom on the snow surface up to a depth of 10 cm. It was then kept frozen at −80 °C in the laboratory until further analysis. A fraction was used for routine microscopic observation (Axio Scope.A1, Zeiss) and allowed for the examination of red spherical cysts, which made up the majority of the bloom. Another aliquot fraction was used to analyze the DNA using Illumina sequencing, i.e., NovaSeq 6000 PE 2x 150 bp. From the data, DNA molecular markers such as internal transcribed spacer (ITS1–ITS2), 18S ribosomal RNA, and plastid rbcL, were analyzed using NCBI BLAST (50). The sequences matched with *S. nivaloides* species. *S. nivaloides* cysts contain colored chlorophylls and a mixture of free and aggregated carotenoids including red astaxanthin glucoside esters (51–53). We used a pellet of 1 million *S. nivaloides* cells for a stepwise extraction of their pigments. An incubation of the cell pellet in 1 mL of acetone 80% in water, v/v, led to a first fraction collected in a supernatant. To ensure complete pigment extraction, the cells were lysed using a Precellys Evolution (Bertin) homogenizer with glass beads (425 to 600 μm, Sigma). The lysis program comprised six homogenization cycles of 30 s at 10,000 rpm and 20-s pauses. The absorption spectrum of this first fraction diluted five times (corresponding to 200,000 cells) was measured from 350 to 750 nm, with a spectrophotometer (Safas) using 80% acetone as a baseline. Peaks corresponding to chlorophyll a (417 nm, 667 nm) and carotenoids (425 to 460 nm) were consistent with a reference mix containing chlorophylls and free carotenoids. A subsequent extraction of the pellet with 1 mL of acetone 80% in water, v/v, with the same procedure, led to a second fraction of all other pigmented molecules, whose absorption spectrum diluted five times (corresponding to 200,000 cells), led to the detection of a broad peak (470 nm) typical of the carotenoid astaxanthin, forming aggregates (*SI Appendix*, Fig. S8). The parameters for snow reflectance simulations were thus selected so that the simulated absorption of the algae matched the absorption of algae measured in the laboratory for *Sanguina* (*SI Appendix*, Fig. S8).

Snow Reflectance Measurements. In this study, we used a collection of snow reflectance spectra measured in the Pyrenees during a clear-sky day (28). The measurements were performed over a snow surface containing mineral dust, algae, or both.

Sentinel-2 Detection Algorithm. Snow and cloud masks (30) were used to identify snow-covered pixels at a 20 m resolution. A rock filter was then applied with band 3 ($R_{green} > 0.5$) (22) to filter darker pixels not eliminated by snow filtering. We used the RGND index (Red Green Normalized Difference) (16, 22) defined as:

$$\text{RGND} = \frac{(R_{red} - R_{green})}{(R_{red} + R_{green})}. \quad [2]$$

The RGND index was used to separate snow containing red algae and pure snow; here, we used a threshold of 0.035 compared to the 0.025 used in a previous study (22), as we aimed to detect only intense blooms.

On account of mineral dust deposition in the Alps and based on the difference in albedo between snow containing algae and dust (e.g., Fig. 1*E*), we introduced the GBND index (Green Blue Normalized Difference), defined as:

$$\text{GBND} = \frac{(R_{green} - R_{blue})}{(R_{green} + R_{blue})}. \quad [3]$$

Pixels were then classified as containing algae or not in the GBND-RGND space. We visually selected 719 pixels of snow containing algae and snow containing dust from satellite images (*SI Appendix*, Fig. S5). The labeled data were separated into two sets (a training set representing 80% of the data, i.e., 575 pixels, and a test set, representing 20% of the data, i.e., 144 pixels). We tested multiple supervised machine learning methods to classify pixels in the GBND-RGND space using scipy in Python, namely, nearest neighbors, linear support vector machine (linear SVM), Gaussian process, decision tree, random forest, and neural network. All methods led to highly similar accuracy values (i.e., higher than 0.99), which was likely due to the explicit separation between the two clusters (*SI Appendix*, Fig. S5). For the sake of readability and to reduce the computational costs of large images, we selected the linear SVM method for detection, which yielded a linear separation in the GBND-RGND space (red solid lines in *SI Appendix*, Fig. S5). We obtained the following linear separation equation with the training set: $\text{RGND} = 1.0057 \times \text{GBND} + 0.0165$. Both thresholds (RGND threshold and linear threshold from the SVM) were then combined to provide binary detection (either algae or not). To avoid as many false-positive cases as possible, a threshold of the size of the connected components was applied to detect only large blooms. Here, we chose a minimum size of 5 with the von Neumann neighborhood (one pixel has four neighbors on a 2D grid). The detection algorithm is summarized in *SI Appendix*, Fig. S6.

Evaluation of the Detection Algorithm. The accuracy of the detection algorithm was first evaluated using simulated spectra from the SNICAR radiative transfer model (see the parameters of the simulations above) and by using snow reflectance values measured in the field from ref. 28. *SI Appendix*, Fig. S7 shows

that for the observed values (triangle markers), nonalgae values were correctly classified, while for the algae values, the two points with the lower algae content were classified as nonalgae and the others were classified correctly. For the simulated spectra (circles), only algae and only dust snow spectra were correctly classified, except for the point with the lowest algae content. For mixed spectra, the algorithm classified as algae the points with more than 50% of an algae fraction and classified the remaining points as nonalgae. We also tested the results of the detection algorithm on simulated spectra when varying other parameters, namely, snow optical radii values between 0.4 and 1.4 mm and solar zenith angle values from 0° to 60°. The results of these sensitivity tests are shown in *SI Appendix*, Fig. S7. In summary, based on the simulated and observed reflectance, we demonstrated that our methodology correctly classified algae spectra with a "sufficiently" high concentration of algae (20,000 cells/mL) and with less than 50% dust (see above for the definition of fractions). It thus limits as much as possible the number of false-positive retrievals, but as a drawback, it does not detect low algae content pixels or pixels with both algae and a large amount of dust.

In addition, we evaluated the algorithm retrievals with in situ observations using six online webcams (*SI Appendix*, Fig. S1). The areas observed by the webcam were located inside one Sentinel-2 pixel. To avoid uncertainties arising from using algorithm detection on only one pixel, we classified this pixel as algae only if more than 50 pixels were detected as algae in the 20 by 20 pixel zone around the webcam location, which we refer to as the "neighborhood zone." If not classified as algae, the pixel was classified as cloud if more than 50 pixels were detected as cloud in the neighborhood zone. If not classified as algae or clouds, the pixel was classified as no algae. The webcam images were manually classified. Namely, for each webcam, 1 or 2 observation areas (centered around the selected pixel) were chosen. In total, we selected nine observation areas. For these images, our visual criterion was that the snow was clearly red (not orange) in the observation area. If we were not sure about the presence of algae, we chose not to classify the webcam image to avoid manual errors. Among 4,608 webcam-classified images, 290 were taken on the exact same day as a noncloudy classified satellite observation. On those dates, considering the webcam images as ground truth, we had the following results: true-negative (TN) = 277, true-positive (TP) = 9, false-positive (FP) = 1, and false-negative (FN) = 3, which leads to an accuracy of 98.6%.

Snowpack Simulations and Dust Deposition Fluxes. Over the French Alps, detailed simulations were performed using the detailed snowpack model SURFEX/ISBA-Crocus with SAFRAN atmospheric reanalysis as inputs (32). Simulations were performed with a 10-y spin-up from 2007 to 2017. Simulations were run from 01-08-2017 to 01-08-2022. The snowpack simulations were performed for flat terrain using a local mask of solar illumination. For the Swiss mountain areas, detailed snowpack simulations were performed using the SNOWPACK model forced with in situ meteorological observations as described in ref. 33.

Those simulations were used to investigate the drivers of the blooms, and were thus run at locations where blooms were detected for more than 1 y. This led to a point approach instead of a regional one. Our objective was to identify as many locations as possible and to sample a region as large as possible. In France, the meteorological and snow data are available at the massif scale and selecting too many points in similar massifs does not provide meaningful information since the meteorological and snow conditions are homogeneous in each massif. In Switzerland, the meteorological and snow data were available at several stations only and we selected all the sites with a large number of bloom retrievals that were also close to a weather station (less than 1 km). As a result, we selected 40 points identified in *SI Appendix*, Fig. S1 (27 points in the French Alps, 13 points in Switzerland). The mean distance between the Swiss selected stations and the points' locations was 595 m (SD 468 m). On average, Swiss stations were 21 m lower than the bloom locations (SD 97 m). The elevations of the 40 simulation points ranged from 2,200 m a.s.l. to 3,000 m a.s.l. In detail, there were 3 points in the range of 2,200 to 2,400 m a.s.l., 16 points in the range of 2,400 to 2,600 m a.s.l., 16 points in the range of 2,600 to 2,800 m a.s.l., and 5 points in the range of 2,800 to 3,000 m a.s.l.

Both snow models simulated similar detailed snow variables, namely, the physical properties of each snow layer, including snow density, temperature, liquid water content, and snow microstructure variables. They have been chosen for their ability in representing the snowpack in their specific alpine region (France and Switzerland). Both have a high performance and have been evaluated thoroughly in several papers (e.g., 54) for several simulated variables. In our study, the snowmelt duration is computed using the snow water equivalent and the "persistence of liquid water" index, defined as the number of days with a fully wet snowpack (when layers containing liquid water account for more than 90% of the snowpack total thickness) between the date of the maximum snow water equivalent and the date of complete melt-out, is computed using the liquid water content. Note that we did not use the absolute value of liquid water content per layer, but an integrated index over the full snow column. Simulated SWE from both Crocus and SNOWPACK has been evaluated in several studies (32, 55–57) with an accuracy of around 50 kg m^{-2}. Evaluations of simulated liquid water content are more sparse due to the spatial heterogeneity of liquid water percolation which is a challenge for both observations and models. However it has been evaluated using in situ observed snow profiles for both models (58, 59) showing reasonable agreement. More recently, liquid water presence simulated by Crocus has been compared to wet snow extent based on remote sensing with the Synthetic Aperture Radar (SAR) of Sentinel-1 satellite (60, 61). Overall, the comparison with Sentinel-1 data demonstrates a good agreement between the simulated and the observed duration of the liquid water presence.

Dust deposition fluxes were obtained from the CNRM-ALADIN63 regional climate model (31), including prognostic aerosols, driven by the ERA5 reanalysis. They were interpolated using a method previously developed and described (24) for the 40 locations of the French and Swiss Alps shown in *SI Appendix*, Fig. S1. We computed the average dust deposition in snow (i.e., the total mass of dust deposition over the annual snow season). Fig. 3*C* shows the normalized mass of dust deposited by location during the snow season (i.e., the depositions at each location are normalized by the mean of the depositions at this location) for years with bloom detection (red) and without bloom detection (black). Depositions have been normalized to account for local effects that might not be represented in the deposition model and ease the comparison between the different locations.

Snowmelt Estimation. As in ref. 11, we estimated snowmelt m_a (kg.m^{-2}) caused by algal blooms as $m_a = \int_{t_s}^{t_e} SW_{down}(t) \cdot D_\alpha \cdot \Delta H_{fus}^{-1} \cdot dt$ with $SW_{down}(t)$ the shortwave incoming radiation, $\Delta H_{fus} = 334$ kJ.kg^{-1} the latent heat of fusion, t_s and t_e the starting and ending date of the bloom, $D_\alpha \in [0.16, 0.35]$ the albedo difference between broadband albedos of snow with algae and pure snow. The range for albedo difference was estimated from SNICAR simulations (27) with algal abundances from 10,000 to 100,000 cells/mL, since the RGND range of these spectra matches the RGND range of the Sentinel-2 pixels labeled as algal blooms (*SI Appendix*, Figs. S5 and S7). Melt estimations were performed for seven intense blooms using the shortwave incoming radiation from SAFRAN reanalysis (see above) at the location and time of the blooms.

For seasonal snow outside glacier area, we estimated the advance of snow melt-out date. This date is computed as the first date of the melt period where the snow water equivalent is lower than the snowmelt caused by algal blooms. Resulting durations were verified using simulations from SURFEX/ISBA-Crocus by lowering snow albedo during the bloom period as described in the paragraph above. The simulations resulted in similar estimations.

Comparing Snowpack Simulations and Algae Detection. For each of the 27 locations in the French Alps shown in *SI Appendix*, Fig. S1, we used the algorithm retrievals and all of the meteorological and snow variables described in *SI Appendix*, Table S1. For each location, combining bloom occurrences and those variables, we sought to determine which variables were correlated with red bloom occurrence, the characteristic time of action of those variables, and whether there was a time shift between the action and the bloom appearance. To perform a statistical analysis, we introduced the following sum of window functions at each location *l*:

$$H_l^d(t) = \frac{1}{\#A} \sum_{y \in A} H_{l,y}^d(t) - \frac{1}{\#A^C} \sum_{y \in A^C} H_{l,y}^d(t), \quad [4]$$

where A is the set of years with bloom detection, A^C is the set of years without bloom detection and $H_{l,y}$ is an indicator function of size d ending at $t_{SMOD,y}$ (snow melt-out date on year y).

The parameter d was introduced here to find the time of action. Next, with n_f, σ_f and $\overline{f}$ being the length, the SD, and the mean of f, we computed the following discrete zero normalized cross-correlation (62) at location l between $H_l^d(t)$ and a variable $V_l(t)$.

$$C_l^d[s] = \frac{1}{n_{V_l} n_{H_l}} \frac{1}{\sigma_{V_l} \sigma_{H_l}} \sum_{t \in T} (V_l[t] - \overline{V_l})(H_l^d[t+s] - \overline{H_l^d}) \qquad [5]$$

T is the set of simulation output times, and s is the shift. The idea is that, for instance, if red blooms were triggered due to high temperatures from exactly 20 to 30 d before the snow melt-out date, the maximum correlation with the temperature variable would be found for $s = 20$ d and $d = 10$ d.

We aggregated the correlations over the 27 locations. Some variables had a higher maximum correlation with bloom retrievals than others (*SI Appendix*, Table S2). High maximum correlations with snow depth and snow water equivalent early in the season highlighted that red blooms were detected during seasons with high snow accumulation. High correlations with variables related to liquid water (wet thickness at the top of the snowpack, runoff, snow melting rate, soil water content) suggested that algal blooms are enhanced by melt and liquid water. This led us to the two indicators used in Fig. 3*A*, i.e., the snowmelt duration and the persistence of liquid water.

Projected Snow Conditions Over the French Alps. The projected maximum snow water equivalent (SWE) and snowmelt duration over the French Alps were derived from statistically adjusted regional climate projections from EURO-CORDEX using the ADAMONT method (63). This method uses a quantile mapping approach, adjusting the quantile distribution of each variable from the RCMs (Regional Climate Models) based on the quantile distribution of a reference dataset, the S2M reanalysis (32) for the French Alps (64). In this study, we used 15 pairs of GCM-RCM, detailed in *SI Appendix*, Table S3, adjusted using the ADAMONT method. The bias-adjusted projections were used to drive the corresponding Crocus snow cover simulations, from which the projected snow conditions were extracted. Projected snow indicators (maximum SWE and snowmelt duration) over the French Alps were computed for 13 massifs that covered the algae proliferation elevation range (thus, simulations were not performed on these 40 points anymore but at a more global scale). A massif is a mountainous area (1,000 km^2 on average) with meteorological conditions considered homogeneous at a given elevation (see ref. 32 for the massif distribution over the French Alps). The historical run was used for the 1970–2005 period, and the projections followed RCP8.5 and RCP4.5, starting in 2005 until the end of the 21st century. Figure 4 shows the projections of the maximum SWE and the projections of the snowmelt duration at 2,400 and 2,700 m a.s.l. The snowmelt duration values are computed as in Fig. 3. *SI Appendix*, Table S4 shows the P-values of the three one-sided tests Pearson, Spearman, and Kendal, computed over 30 y (30 values), with the null hypothesis being an absence of decrease and the alternative hypothesis being a decrease of the variable.

Online Map of Algal Blooms. The red contours of the online map were built from the raster, which counts the number of retrievals, then downsampled and smoothed with a Gaussian kernel.

Data, Materials, and Software Availability. The detection algorithm used in this study is available at https://doi.org/10.5281/zenodo.10208773 (65). Surface reflectance and snow cover products are freely distributed by Theia over the studied region at https://theia.cnes.fr/atdistrib/rocket/#/home (66). Snowpack simulations, dust simulations, and algae absorptions are available at https://doi.org/10.5281/zenodo.10210416 (67). An online heatmap showing the intense bloom regions is available at http://u.osmfr.org/m/936611/ (68) (see *Materials and Methods* for the processing).

ACKNOWLEDGMENTS. We are grateful to Yannick Deliot, Olivier Mestre, Florent Domine, Kevin Fourteau, Anne Dufour, Fatima Karbou, Ghislain Picard, Bruno Jourdain, and Bertrand Cluzet for their help during the realization of this study. Centre Nationale Recherches Météorologiques, Centre d'Étude de la Neige and Institut des Géosciences de l'Environnement are part of Labex OSUG@2020. Laboratoire Physiologie Cellulaire et Végétale is part of Labex Grenoble Alliance for Integrated Structural and Cell Biology (ANR-10-LABX-49-01). This work was funded by the French Space Agency (Centre National d'Études Spatiales) Appel à Propositions de Recherche (MountaIns ObServatiOns and simulaTIons of Snow project), and Agence Nationale de la Recherche (ALPALGA project; Grant No. ANR-20-CE02-0020). *S. nivaloides* bloom analyses were performed with the support of the Kilian Jornet Foundation. This research has been supported by the European Research Council under the European Union's Horizon 2020 Research and Innovation Program (IVORI project, standing for New insights on the snow cover : from snowflakes to ice sheets, in seconds to centuries; Grant No. 949516).

Author affiliations: [a]Centre d'Études de la Neige, Université Grenoble Alpes, Université de Toulouse, Météo-France, CNRS, Centre Nationale Recherches Météorologiques (CNRM), Grenoble 38000, France; [b]Centre d'Études Spatiales de la Biosphère (CESBIO), Université de Toulouse, Toulouse 31000, France; [c]Institut für Schnee und Lawinenforschung (SLF), Forschungsanstalt für Wald, Schnee und Landschaft (WSL), Davos Dorf 7260, Switzerland; [d]Centre Nationale Recherches Météorologiques (CNRM), Université de Toulouse, Météo-France, CNRS, Toulouse 31000, France; and [e]Laboratoire de Physiologie Cellulaire et Végétale (LPCV), Université Grenoble Alpes, CNRS, Commissariat á l'Énergie Atomique et aux Énergies Alternatives (CEA), Institut National de la Recherche Agronomique (INRA), Grenoble 38000, France

Author contributions: L.R., M.D., and S.G. designed research; L.R., M.D., S.G., and D.M. performed research; L.R., M.D., S.G., D.M., M.B., P.N., J.A.E., M.F., M.L., and E.M. analyzed data; and L.R., M.D., and S.M. wrote the paper.

1. R. W. Hoham, D. Remias, Snow and glacial algae: A review. *J. Phycol.* **56**, 264–282 (2020).
2. T. Segawa *et al.*, Bipolar dispersal of red-snow algae. *Nat. Commun.* **9**, 3094 (2018).
3. T. Suzuki, N. Takeuchi, Influence of vegetation on occurrence and color of snow algal blooms in Mt. Gassan, Yamagata Prefecture, Japan. *Arctic, Antarctic Alp. Res.* **55**, 2173138 (2023).
4. B. Di Mauro *et al.*, Glacier algae foster ice-albedo feedback in the European Alps. *Sci. Rep.* **10**, 4739 (2020).
5. A. Stewart *et al.*, Altitudinal zonation of green algae biodiversity in the French Alps. *Front. Plant Sci.* **12**, 679428 (2021).
6. J. A. Ezzedine *et al.*, Adaptive traits of cysts of the snow alga *Sanguina nivaloides* unveiled by 3D subcellular imaging. *Nat. Commun.* **14**, 7500 (2023).
7. S. Lutz *et al.*, The biogeography of red snow microbiomes and their role in melting Arctic Glaciers. *Nat. Commun.* **7**, 11968 (2016).
8. S. M. Skiles, M. Flanner, J. M. Cook, M. Dumont, T. H. Painter, Radiative forcing by light-absorbing particles in snow. *Nat. Clim. Change* **8**, 964–971 (2018).
9. L. G. Benning, A. M. Anesio, S. Lutz, M. Tranter, Biological impact on Greenland's albedo. *Nat. Geosci.* **7**, 691 (2014).
10. L. Halbach *et al.*, Dark ice in a warming world: Advances and challenges in the study of Greenland ice sheet's biological darkening. *Ann. Glaciol.* **63**, 95–100 (2023).
11. C. B. Engstrom, L. M. Quarmby, Satellite mapping of red snow on North American Glaciers. *Sci. Adv.* **9**, eadi3268 (2023).
12. T. L. Hamilton, J. Havig, Primary productivity of snow algae communities on stratovolcanoes of the Pacific Northwest. *Geobiology* **15**, 280–295 (2017), 10.1111/gbi.12219.
13. K. Kobayashi, N. Takeuchi, M. Kagami, High prevalence of parasitic chytrids infection of glacier algae in cryoconite holes in Alaska. *Sci. Rep.* **13**, 3973 (2023).
14. A. E. Tucker, S. P. Brown, Sampling a gradient of red snow algae bloom density reveals novel connections between microbial communities and environmental features. *Sci. Rep.* **12**, 10536 (2022).
15. T. H. Painter *et al.*, Detection and quantification of snow algae with an airborne imaging spectrometer. *Appl. Environ. Microbiol.* **67**, 5267–5272 (2001).
16. G. Ganey, M. Loso, A. Burgess, R. Dial, The role of microbes in snowmelt and radiative forcing on an Alaskan Icefield. *Nat. Geosci.* **10**, 754–759 (2017).
17. A. Gray *et al.*, Remote sensing reveals Antarctic green snow algae as important terrestrial carbon sink. *Nat. Commun.* **11**, 2527 (2020).
18. J. McCutcheon *et al.*, Mineral phosphorus drives glacier algal blooms on the Greenland ice sheet. *Nat. Commun.* **12**, 570 (2021).
19. C. M. Phillips-Lander *et al.*, Snow algae preferentially grow on Fe-containing minerals and contribute to the formation of Fe phases. *Geomicrobiol. J.* **37**, 572–581 (2020).
20. Y. Dai *et al.*, Coastal phytoplankton blooms expand and intensify in the 21st century. *Nature* **615**, 280–284 (2023).
21. N. Takeuchi, R. Dial, S. Kohshima, T. Segawa, J. Uetake, Spatial distribution and abundance of red snow algae on the Harding Icefield, Alaska derived from a satellite image. *Geophys. Res. Lett.* **33**, L21502 (2006), 10.1029/2006GL027819.
22. C. B. Engstrom, S. N. Williamson, J. A. Gamon, L. M. Quarmby, Seasonal development and radiative forcing of red snow algal blooms on two glaciers in British Columbia, Canada, Summer 2020. *Remote. Sens. Environ.* **280**, 113164 (2022).
23. C. Xue-Yang, S. Shuang-Lin Li, C. Zhang, L. Dong-Yan, Snow algal blooms in Antarctic King George Island in 2017–2022 and their future trend based on CMIP6 projection. *Adv. Clim. Change Res.* **14**, 732–745 (2023).

24. M. Reveillet *et al.*, Black carbon and dust alter the response of mountain snow cover under climate change. *Nat. Commun.* **13**, 5279 (2022).
25. B. Di Mauro *et al.*, Saharan dust events in the European Alps: Role in snowmelt and geochemical characterization. *Cryosphere* **13**, 1147–1165 (2019).
26. B. Di Mauro *et al.*, Combined effect of algae and dust on snow spectral and broadband albedo. *J. Quant. Spectrosc. Radiat. Transf.* **316**, 108906 (2024).
27. M. G. Flanner *et al.*, SNICAR-ADv3: A community tool for modeling spectral snow albedo. *Geosci. Model. Dev.* **14**, 7673–7704 (2021).
28. J. Pey *et al.*, Snow impurities in the central pyrenees: From their geochemical and mineralogical composition towards their impacts on snow albedo. *Atmosphere* **11**, 937 (2020).
29. M. Drusch *et al.*, Sentinel-2: ESA's optical high-resolution mission for GMES operational services. *Remote Sens. Environ.* **120**, 25–36 (2012).
30. S. Gascoin, M. Grizonnet, M. Bouchet, G. Salgues, O. Hagolle, Theia Snow collection: High-resolution operational snow cover maps from Sentinel-2 and Landsat-8 data. *Earth Syst. Sci. Data* **11**, 493–514 (2019).
31. P. Nabat *et al.*, Modulation of radiative aerosols effects by atmospheric circulation over the Euro-Mediterranean region. *Atmos. Chem. Phys.* **20**, 8315–8349 (2020).
32. M. Vernay *et al.*, The S2M meteorological and snow cover reanalysis over the French mountainous areas: Description and evaluation (1958–2021). *Earth Syst. Sci. Data* **14**, 1707–1733 (2022).
33. S. Morin *et al.*, Application of physical snowpack models in support of operational avalanche hazard forecasting: A status report on current implementations and prospects for the future. *Cold Reg. Sci. Technol.* **170**, 102910 (2020).
34. T. H. Painter *et al.*, Detection and quantification of snow algae with an airborne imaging spectrometer. *Appl. Environ. Microbiol.* **67**, 5267–5272 (2001).
35. B. Grinde, Vertical distribution of the snow alga *Chlamydomonas nivalis* (Chlorophyta, Volvocales). *Polar Biol.* **2**, 159–162 (1983).
36. T. L. Torsten Müller, G. Fuhr, Persistent snow algal fields in Spitsbergen: Field observations and a hypothesis about the annual cell circulation. *Arctic, Antarctic, Alp. Res.* **33**, 42–51 (2001).
37. L. Procházková, T. Leya, H. Křížková, L. Nedbalová, *Sanguina nivaloides* and *Sanguina aurantia* gen. et spp. nov. (Chlorophyta): The taxonomy, phylogeny, biogeography and ecology of two newly recognised algae causing red and orange snow. *FEMS Microbiol. Ecol.* **95**, fiz064 (2019).
38. M. Marcer *et al.*, Permafrost favorability index: Spatial modeling in the French alps using a rock glacier inventory. *Front. Earth Sci.* **5**, 105 (2017).
39. M. Dumont *et al.*, Spatial variability of Saharan dust deposition revealed through a citizen science campaign. *Earth Syst. Sci. Data* **15**, 3075–3094 (2023).
40. M. Dumont *et al.*, Accelerated snow melt in the Russian Caucasus mountains after the Saharan dust outbreak in March 2018. *J. Geophys. Res. Earth Surf.* **125**, e2020JF005641 (2020).
41. A. Gray *et al.*, Remote sensing phenology of Antarctic green and red snow algae using worldview satellites. *Front. Plant Sci.* **12**, 671981 (2021).
42. K. N. Musselman, M. P. Clark, C. Liu, K. Ikeda, R. Rasmussen, Slower snowmelt in a warmer world. *Nat. Clim. Change* **7**, 214–219 (2017).
43. O. Hagolle, M. Huc, D. Villa Pascual, G. Dedieu, A multi-temporal and multi-spectral method to estimate aerosol optical thickness over land, for the atmospheric correction of FormoSat-2, LandSat, VENμS and Sentinel-2 images. *Remote Sens.* **7**, 2668–2691 (2015).
44. O. Hagolle, M. Huc, D. V. Pascual, G. Dedieu, A multi-temporal method for cloud detection, applied to FORMOSAT-2, VENμS, LANDSAT and SENTINEL-2 images. *Remote Sens. Environ.* **114**, 1747–1755 (2010).
45. S. Skakun *et al.*, Cloud Mask Intercomparison eXercise (CMIX): An evaluation of cloud masking algorithms for Landsat 8 and Sentinel-2. *Remote Sens. Environ.* **274**, 112990 (2022).
46. J. Colin *et al.*, Assessment of the performance of the atmospheric correction algorithm MAJA for Sentinel-2 surface reflectance estimates. *Remote Sens.* **15**, 2665 (2023).
47. Z. Barrou Dumont *et al.*, Brief communication: Evaluation of the snow cover detection in the Copernicus High Resolution Snow Ice Monitoring Service. *Cryosphere* **15**, 4975–4980 (2021).
48. AlpineConvention, Perimeter of the Alpine Convention. Alpine Convention Atlas. https://www.atlas.alpconv.org/layers/geonode_data:geonode:Alpine_Convention_Perimeter_2018_v2. Deposition 20 July 2020.
49. J. M. Cook *et al.*, Quantifying bioalbedo: A new physically based model and discussion of empirical methods for characterising biological influence on ice and snow albedo. *Cryosphere* **11**, 2611–2632 (2017).
50. S. F. Altschul, W. Gish, W. Miller, E. W. Myers, D. J. Lipman, Basic local alignment search tool. *J. Mol. Biol.* **215**, 403–410 (1990).
51. T. Řezanka, L. Nedbalová, K. Sigler, V. Cepák, Identification of astaxanthin diglucoside diesters from snow alga *Chlamydomonas nivalis* by liquid chromatography-atmospheric pressure chemical ionization mass spectrometry. *Phytochemistry* **69**, 479–490 (2008).
52. T. Řezanka, L. Nedbalová, I. Kolouchová, K. Sigler, LC-MS/APCI identification of glucoside esters and diesters of astaxanthin from the snow alga *Chlamydomonas nivalis* including their optical stereoisomers. *Phytochemistry* **88**, 34–42 (2013).
53. D. Remias, M. Pichrtová, M. Pangratz, C. Lütz, A. Holzinger, Ecophysiology, secondary pigments and ultrastructure of *Chlainomonas* sp. (Chlorophyta) from the European Alps compared with *Chlamydomonas nivalis* forming red snow. *FEMS Microbiol. Ecol.* **92**, fiw030 (2016).
54. C. B. Menard *et al.*, Scientific and human errors in a snow model intercomparison. *Bull. Am. Meteorol. Soc.* **102**, E61–E79 (2021).
55. V. Vionnet *et al.*, The detailed snowpack scheme crocus and its implementation in SURFEX v7.2. *Geosci. Model. Dev.* **5**, 773–791 (2012).
56. E. Schmucki, C. Marty, C. Fierz, M. Lehning, Simulations of 21st century snow response to climate change in Switzerland from a set of RCMs. *Int. J. Climatol.* **35**, 3262–3273 (2015), https://onlinelibrary.wiley.com/doi/pdf/10.1002/joc.4205.
57. M. Lafaysse *et al.*, A multiphysical ensemble system of numerical snow modelling. *Cryosphere* **11**, 1173–1198 (2017).
58. N. Wever *et al.*, Verification of the multi-layer SNOWPACK model with different water transport schemes. *Cryosphere* **9**, 2271–2293 (2015).
59. L. Viallon-Galinier, P. Hagenmuller, M. Lafaysse, Forcing and evaluating detailed snow cover models with stratigraphy observations. *Cold Reg. Sci. Technol.* **180**, 103163 (2020).
60. F. Karbou, G. James, M. Fructus, F. Marti, On the evaluation of the SAR-based Copernicus snow products in the French Alps. *Geosciences* **12**, 420 (2022).
61. C. Turbé, F. Karbou, A. Rabatel, I. Gouttevin, "Snowmelt dynamics in a temperate glacier using Sentinel-1 SAR images: A case study on Saint-Sorlin Glacier, French Alps" in *IEEE Journal of Selected Topics in Applied Earth Observations and Remote Sensing* (2024), pp. 1–15.
62. B. Podobnik, D. Wang, D. Horvatic, I. Grosse, H. E. Stanley, Time-lag cross-correlations in collective phenomena. *Europhys. Lett.* **90**, 68001 (2010).
63. D. Verfaillie, M. Déqué, S. Morin, M. Lafaysse, The method ADAMONT v1.0 for statistical adjustment of climate projections applicable to energy balance land surface models. *Geosci. Model. Dev.* **10**, 4257–4283 (2017).
64. D. Verfaillie *et al.*, Multi-component ensembles of future meteorological and natural snow conditions for 1500 m altitude in the Chartreuse Mountain Range, Northern French Alps. *Cryosphere* **12**, 1249–1271 (2018).
65. L. Roussel *et al.*, Code for teledetection of red algal blooms in the European Alps using Sentinel-2 images. Zenodo. https://doi.org/10.5281/zenodo.10208773. Deposited 27 November 2023.
66. Theia, Centre National d'Études Spatiales, Muscate Atelier de Distribution. Theia. https://theia.cnes.fr/atdistrib/rocket/#/home. Accessed 27 November 2023.
67. L. Roussel *et al.*, Data used to identify drivers of red algal blooms in the European Alps. Zenodo. https://doi.org/10.5281/zenodo.10210416. Deposited 27 November 2023.
68. L. Roussel, Map of red algae in alpine snow. Umap OpenStreepMap France. http://u.osmfr.org/m/936611/. Deposited 27 November 2023.